

# Compact Optical Antenna Coupler for Silicon Photonics Characterized by Third-Harmonic Generation

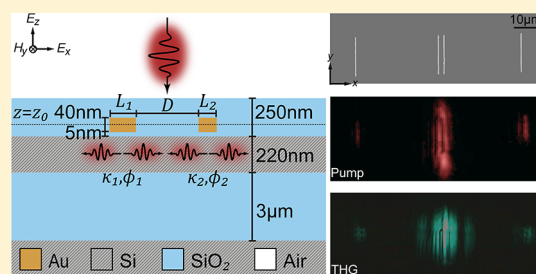
Themistoklis P. H. Sidiropoulos,<sup>†,§</sup> Michael P. Nielsen,<sup>†,§</sup> Tyler R. Roschuk,<sup>†</sup> Anatoly V. Zayats,<sup>‡</sup> Stefan A. Maier,<sup>†</sup> and Rupert F. Oulton<sup>\*,†</sup>

<sup>†</sup>Department of Physics, Imperial College London, London, SW7 2AZ, U.K.

<sup>‡</sup>Department of Physics, King's College London, Strand, London WC2R 2LS, U.K.

**ABSTRACT:** We exploit the strong interaction between a focused free-space beam and an optical antenna to construct a compact and efficient silicon waveguide coupler operating simultaneously in several telecommunications bands. The antenna is a directional coupler tuned by the spacing and relative size of its two constituent nanoparticles. Moreover, the antenna's compact size and short scattering lifetime provide a bandwidth sufficient to couple 200 fs pulses at both 1500 and 1350 nm simultaneously. By measuring the third-harmonic generation (THG) from waveguide-coupled light we verify our estimates of the high in-coupling efficiency of these antennas. Coupling efficiencies were estimated to be as high as 19% and 14% at the wavelengths of 1500 and 1350 nm, respectively.

**KEYWORDS:** nano-optics, silicon photonics, plasmonics, nonlinear optics, third-harmonic generation



The strong interaction of light with electrons at metal interfaces allows for extreme confinement of light, enabling strongly enhanced light–matter interactions<sup>1,2</sup> beyond the intrinsic capabilities of the underlying materials. While many researchers have proposed to enhance the electromagnetic field through confinement,<sup>3</sup> surface electromagnetic excitations at metal nanoparticles, known as localized surface plasmons<sup>4</sup> (LSPs), also present extremely strong extinction cross sections to free-space beams. LSPs have been successfully exploited to control the directionality of light<sup>5–8</sup> and in particular have found applications in light trapping for photovoltaics.<sup>9</sup> In addition, strong coupling between nanoparticles and adjacent waveguides has been extensively utilized to modify the transmission through the nearby waveguides.<sup>10–12</sup> In this Letter, we use this capability of metallic nanoparticles to effectively and directionally scatter light from a focused free-space beam into a silicon-on-insulator (SOI) waveguide, following an earlier theoretical proposal.<sup>13</sup> Similar approaches have been taken to directionally launch surface plasmon polaritons (SPPs) on a metal sheet using either slits<sup>14</sup> or dielectric cavities.<sup>15</sup> Nanoparticles are placed in close proximity to a suitably sized silicon waveguide, which establishes a rapid scattering channel into the waveguide's fundamental mode. The additional scattering into the waveguide also diminishes the effect of ohmic loss, which typically limits plasmonic applications, and we report ~20% coupling efficiencies despite the very small footprint of the coupler of 755 nm.

With this high coupling efficiency and small footprint, nanoparticle waveguide couplers also avoid other drawbacks of commonly used coupling schemes. While simple gratings also have coupling efficiencies of ~20%,<sup>16</sup> they must be relatively

large and ultimately are limited by the dispersive link between the coupling wavelength and the incident beam angle. This limitation establishes an efficiency to bandwidth trade-off that is insufficient for many applications requiring either multiple wavelengths across different communications bands or ultrashort pulses. Prism couplers provide greater coupling efficiency but are also limited by the same wavelength-angle sensitivity as gratings. Consequently many commercial products and researchers utilize end-fire coupling, which generally requires extensive postprocessing and, in its most common implementation, suffers from coupling efficiencies as low as 1%.<sup>17–19</sup> Meanwhile, the extremely fast radiative processes in nanoparticle-based couplers provide broadband operation with very low group delay dispersion.<sup>13</sup> The high coupling efficiency and low dispersion of our couplers preserve the high field intensities of the short pulses, allowing us to estimate the coupling efficiency from the third-harmonic-generation signals.

The coupler is an optical nanoantenna formed by two metallic gold nanoparticles placed on top of a SOI slab waveguide into which light is launched, shown schematically in Figure 1a. The Au nanoparticles were fabricated on a SOI substrate coated with 5 nm of SiO<sub>2</sub> using electron beam lithography patterning followed by the sputtering of 40 nm of Au and then by a lift-off process. Separating the antenna from the silicon waveguide by 5 nm and coating with a further 250 nm of SiO<sub>2</sub> provide a uniform local environment for stronger plasmonic particle resonances. The position of the antenna close to the silicon waveguide also ensures a strong overlap of the nanoparticle's resonance with the transverse magnetic

Received: July 30, 2014

Published: September 17, 2014

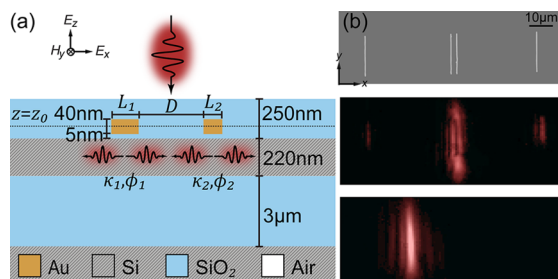


**Figure 1.** (a) Schematic of the realized device, along with (b) SEM images of the couplers (top) with an IR camera image depicting coupling when the input beam is on (middle) and off (bottom) the in-coupler.

(TM) waveguide mode. Moreover, the Si waveguide thickness was chosen to be 220 nm, in order to maximize this interaction.<sup>13</sup>

In order to verify the effectiveness of the antenna, out-coupler antennas consisting of single-particle plasmonic resonators were placed on either side of the in-coupler and displaced by 35  $\mu\text{m}$ . A top view SEM image of the complete structure showing in- and out-coupler antennas is presented in Figure 1b. The infrared (IR) camera images show the coupling when a TM-polarized (along the  $x$ -direction) input beam is on and off the in-coupler, respectively. When the incident beam is off the in-coupler, there is no coupling to the waveguide, and no light is observed at either out-coupler. The width-dependent resonance of each plasmonic nanoparticle coupler determines its response to the incident focused light and the coupling to the waveguide mode. Even though the particles also extend 15  $\mu\text{m}$  in the  $y$ -direction, they effectively generate a TM mode propagating along the  $x$ -direction with very little diffraction in the  $y$ -direction, allowing us to describe the system using a 2-D model. Here, the length of the particles was chosen to facilitate experiments but can be easily downscaled to even match the length of a diffraction-limited input spot without significantly affecting the antenna's properties. Such small couplers, however, would cause diffraction of the coupled modes in the plane; thus the nanoparticles should be placed directly on a ridge waveguide with transport in only a single dimension,<sup>10–12</sup> which would also illicit control over the launched polarization or indeed provide nonlinear switching capabilities.<sup>20</sup> We note that the chosen arrangement is merely a simplification, and our approach can be readily adapted to more complex nanoparticle geometries coupled to 2-D silicon waveguides. Our design here uses two plasmonic particles so that variation of their relative width and separation controls the interference of scattered light into the waveguide and thus the degree of directional coupling.

Transmission into the forward and backward  $x$ -directions from a nanoparticle optical antenna can be modeled in 2-D as two forced coupled dipoles. The interference of their emitted radiation is given by<sup>13</sup>

$$t_{\pm} = (\kappa_1 \kappa_2 e^{\pm i\psi}) \begin{bmatrix} \gamma_1 \omega / \cos \phi_1 e^{-i\phi_1} & -i\kappa_2 \kappa_1 e^{-i\psi} \\ -i\kappa_1 \kappa_2 e^{-i\psi} & \gamma_2 \omega / \cos \phi_2 e^{-i\phi_2} \end{bmatrix}^{-1} \begin{pmatrix} c_1 \\ c_2 \end{pmatrix} \quad (1)$$

where  $c_i$  are the coupling rates between the input laser beam and the LSPs,  $\gamma_i$  are the LSP extinction rates, and  $\kappa_i$  are the coupling coefficients between the waveguide mode and the particles' LSPs. These parameters are simply controlled by adjusting the nanoparticle's width,  $L_i$ . In this harmonic

oscillator model, the off-diagonal components account for the multiple scattering effects. The phase difference between the particles' scattering is described by  $\Delta = \phi_2 - \phi_1$ , and the relative phase  $\psi$  from the propagation between the two particles is determined by the wavevector and the particle spacing through  $\psi = kD$ . This leads to optimal coupling when  $\Delta + \psi = 2\pi n$ , where  $n$  is an integer. However, in our earlier theoretical work we noted that multiple scattering is extremely strong in this system and that this implies that optimum directionality does not imply optimal coupling efficiency.<sup>13</sup> Furthermore, the reader should note optimum directional coupling depends on both the wavelength and the particle spacing.

In order to measure the coupler's directionality and efficiency, we excite the particle pair as shown in Figure 1b and measure the transmitted signals at the left ( $I_l$ ) and right ( $I_r$ ) out-couplers using an IR camera. The signals are then normalized to the reflected signal from the SOI substrate ( $I_{\text{SOI}}$ ). For example, the reflectivity of SOI at 1500 nm was calculated by referencing against the reflected signal from a 40 nm thick gold patch ( $I_{\text{Au}}$ ) with a simulated thin-film reflectivity of  $\rho_{\text{Au}} = 94\%$ , so that  $\rho_{\text{SOI}} = \rho_{\text{Au}} I_{\text{SOI}} / I_{\text{Au}} = 25\%$ . The combined directional transmission or coupling efficiency  $\eta_{C(\text{lr})}$  through the entire structure was then calculated as  $\eta_{C(\text{lr})} = \rho_{\text{SOI}} I_{(\text{lr})} / I_{\text{SOI}}$ . We first identified the maximum directional transmission at 1500 nm from a sample of antennas with varying widths ( $L_1$  and  $L_2$ ) and particle spacing ( $D$ ). An asymmetric particle pair of  $L_1 = 305$  nm and  $L_2 = 200$  nm was found to be optimal. At this point we measured the variation in directional transmission as a function of the particle spacing for symmetric ( $L_1 = L_2 = 305$  nm) and asymmetric ( $L_1 = 305$  nm and  $L_2 = 200$  nm) antennas, shown in Figures 2a and b, respectively. This illustrates the directionality of the antenna due to the phase difference,  $\Delta$ ,

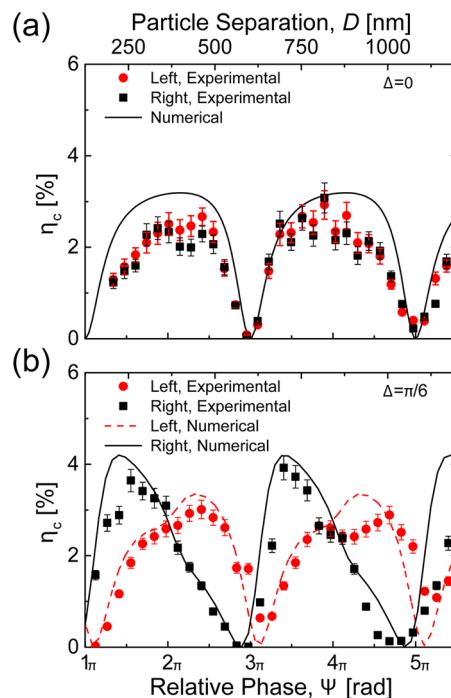


**Figure 2.** Normalized out-coupled power measured as a function of relative phase  $\psi$  and interparticle separation  $D$  between nanoparticles at  $\lambda = 1500$  nm for the (a)  $L_1 = L_2 = 305$  nm symmetric and (b)  $L_1 = 305$  nm and  $L_2 = 200$  nm asymmetric antennas depicting directional coupling as compared to a harmonic oscillator model.

between its constituent nanoparticles as well as the interparticle distance,  $D$ , and their relative phase,  $\psi$ . The observed experimental variation with  $\psi$  agrees well with our harmonic oscillator model, which accounts for multiple scattering between nanoparticles. Although the asymmetric antenna has a peak transmission of  $3.6 \pm 0.2\%$  at  $D = 250$  nm, the in-coupling efficiency cannot be determined as the out-coupling efficiency remains unknown.<sup>16,21,22</sup> In simulations we calculate an out-coupler efficiency of 19.4% at 1500 nm, and so we estimate that our maximum in-coupling efficiency is  $19 \pm 1\%$  for this asymmetric coupler. Later in this work, we support this far-field estimate using a nonlinear technique probing the near field.

In order to verify the broadband nature of the antenna couplers, the variation of  $\eta_{C(L_1)}$  with wavelength was measured using a supercontinuum source ranging from 1 to 1.6  $\mu\text{m}$ . Figure 3 depicts the transmission spectra of the symmetric and

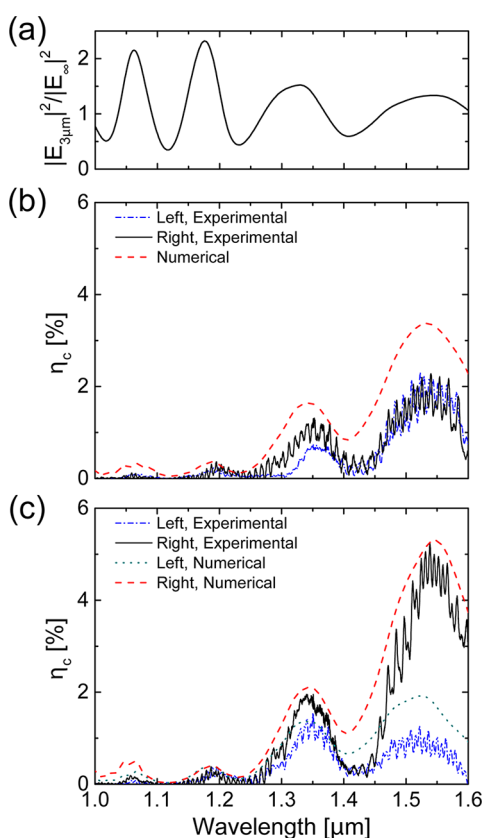


**Figure 3.** (a) Calculated  $|E|^2$  at  $z = z_0$  in the center of the in-coupler depicting the modulation from the 3  $\mu\text{m}$  buried oxide layer and normalized to the case of infinite buried oxide. Broadband white light measurements for the (b)  $L_1 = L_2 = 305$  nm with  $D = 250$  nm symmetric antenna and the (c)  $L_1 = 305$  nm and  $L_2 = 200$  nm with  $D = 250$  nm asymmetric antenna.

asymmetric antennas with  $D = 250$  nm. From the calculated out-coupling efficiencies of 19.4% and 13.9% at 1500 and 1350 nm, respectively, we estimate the in-coupling efficiency of the asymmetric coupler to be  $19 \pm 2\%$  at 1500 nm and  $14 \pm 1\%$  at 1350 nm. When compared to numerical calculations, the results show good correspondence. The numerical calculations presented here are based on those utilized in our previous theoretical proposal,<sup>13</sup> but now take into account the finite buried oxide layer thickness. The various modulations seen in

the experimental data are associated with focused beam interference due to reflections from the buried oxide/silicon substrate interface and modal reflections between the in- and out-couplers. The low-frequency oscillations are attributed to substrate interference of the input beam, which modulates the electric field strength at the position of the antenna (Figure 3a), thus affecting the scattering into the waveguide. The high-frequency oscillations are Fabry–Pérot interference of coupled light between the antennas. A Fourier transform of the data shows peaks associated with propagation distances of  $2.9 \pm 0.1$   $\mu\text{m}$  in  $\text{SiO}_2$  and  $34 \pm 1$   $\mu\text{m}$  in a TM-polarized Si slab mode, corresponding to the buried oxide layer thickness of 3  $\mu\text{m}$  and the interantenna spacing of 35  $\mu\text{m}$ . From the Fourier transform, we can also extract the approximate strength of these reflections. The reflectivities of  $24 \pm 2\%$  for the buried oxide/silicon substrate interface and  $4.4 \pm 0.8\%$  for the cavity between the antennas are in good agreement with the numerical calculations. The numerical model presented here does not include the reflections between the antennas for better clarity of presentation. Despite the strong substrate interference, the results are in good agreement with previously published numerical results and allow broadband coupling across the near-infrared. Engineering of the buried oxide/substrate interface can eliminate unwanted reflections in order to recover the underlying broad coupling bandwidth of these antennas.

Since these couplers are capable of efficiently coupling light over a broad range of wavelengths, they can couple short pulses of light without significant broadening or dispersion. We exploit this to verify our estimate of the in-coupling efficiency seen in Figures 2 and 3, without relying on a calculated out-coupling efficiency, by using third-harmonic generation (THG) at the antenna couplers. Since THG is strongly dependent on the near-field intensity at the antennas, this method provides a verification of the above estimated coupling efficiency. As depicted in Figure 4a, 200 fs FWHM pulses at either 1500 or 1350 nm are aligned to the in-coupler, and the THG signal is selectively measured in a spectrometer from the in- and out-couplers using an aperture, with the reference signal taken from the bare silicon interface. Since silicon strongly absorbs below 1100 nm, the THG signals seen at the out-coupler ( $I_{\text{in}}^{\text{THG}}$ ) must be directly related to the local field intensity of the fundamental signal in the Si at the out-coupler. By comparing these to a reference THG signal from the silicon interface ( $I_0^{\text{THG}}$ ), we can estimate the ratio of near-field intensity in the waveguide relative to the input beam,  $\Pi$ , where

$$\Pi = \left( \frac{I_{\text{in}}^{\text{THG}}}{I_0^{\text{THG}}} \right)^{1/3} \quad (2)$$

Interestingly, measuring  $\Pi$  provides a verification of our previous estimates of the coupling efficiency. We note that it is not a direct measure of the true coupling efficiency, as the local field enhancement and third-harmonic scattering to the far field are unknown. Further investigation into the link between  $\Pi$  and the true coupling efficiency is outside the scope of this Letter.

Figure 4b shows the linear input power dependence of the cubic root of the THG signals from bare silicon, the in-coupler, and the out-coupler for the asymmetric antenna.  $\Pi$  as a function of the input intensity for both 1500 and 1350 nm is shown in Figure 4c. By a linear extrapolation to zero pump power we find  $\Pi$  to be  $25.5 \pm 0.8\%$  and  $18.6 \pm 0.6\%$  for the wavelengths of 1500 and 1350 nm, respectively. These support

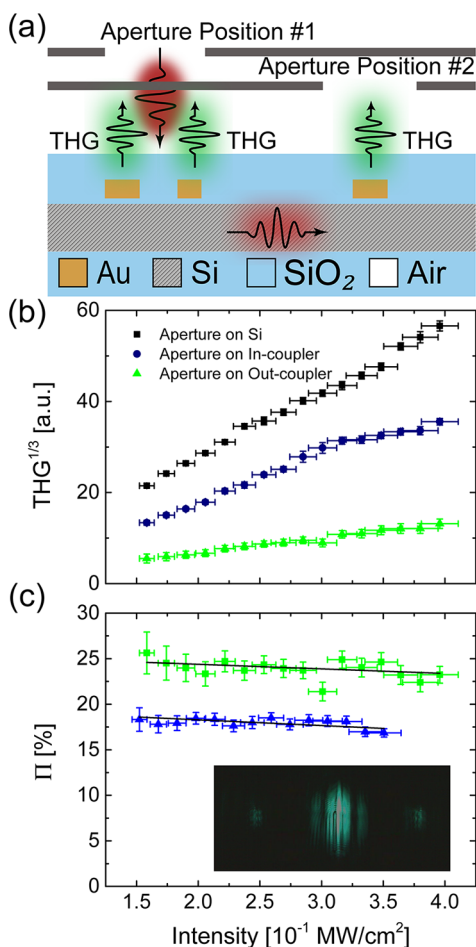


**Figure 4.** (a) Schematic for the THG measurements at the in-coupler (aperture position #1) and out-coupler measurements at the in-coupler (aperture position #1) and out-coupler (aperture position #2). (b) THG measurements at 1500 nm on the  $L_1 = 305$  nm and  $L_2 = 200$  nm with  $D = 250$  nm asymmetric antenna and (c)  $\Pi$  at 1500 nm (squares) and 1350 nm (triangles), with the inset showing a camera image of the THG signal at  $\lambda = 1500$  nm taken at the highest pump intensity.

our estimates of the coupling efficiencies from linear measurements combined with simulations at both of these wavelengths. The small linear dependence on input intensity of  $\Pi$  is most likely due to two-photon absorption.<sup>23</sup> In addition, as we are using short femtosecond pulses at a sufficiently low repetition rate, we can safely ignore the effects of free-carrier absorption. The 80 MHz repetition rate of our laser corresponds to a temporal spacing of 12.5 ns between pulses, which is much larger than the  $\sim 1$  ns free carrier recombination time in silicon.<sup>24</sup>

In conclusion, compact plasmonic–photonic antennas are presented that can couple free-space radiation into silicon waveguide modes with high efficiency and directionality over multiple telecommunications bands. The measured directionality nicely follows the predictions of a harmonic oscillator model, suggesting strong multiple scattering effects between nanoparticles, which is a byproduct of the efficient coupling.<sup>13</sup> Despite the transmission modulation due to input beam interference within the buried oxide layer, the bandwidth remains broad enough to couple 200 fs pulses into the waveguide at the distinct wavelengths of 1500 and 1350 nm. We estimated the coupling efficiencies to be as high as 19% and 14% at 1500 and 1350 nm, respectively, which we also verified with THG measurements. Clearly, these high coupling

efficiencies demonstrate that the antenna rapidly radiates into the silicon waveguide. The large bandwidth and low dispersion of this coupling scheme makes it useful for photonic integrated circuits (PICs), which require the coupling of short femtosecond pulses for ultrafast processes. As the integration density on PICs continues to increase, couplers with compact device footprints, such as this one, will become ever more important.

## AUTHOR INFORMATION

### Corresponding Author

\*E-mail: r.oulton@imperial.ac.uk

### Author Contributions

<sup>§</sup>T. P. H. Sidiropoulos and M. P. Nielsen contributed equally to this work.

### Notes

The authors declare no competing financial interest.

## ACKNOWLEDGMENTS

This work was sponsored by the UK Engineering and Physical Sciences Research Council (EPSRC) and the Natural Sciences and Engineering Research Council of Canada (NSERC). R.F.O. is supported by an EPSRC Fellowship (EP/I004343/1) and Marie Curie IRG (PIRG08-GA-2010-277080).

## REFERENCES

- (1) Anger, P.; Bharadwaj, P.; Novotny, L. Enhancement and Quenching of Single-Molecule Fluorescence. *Phys. Rev. Lett.* **2006**, *96*, 113002.
- (2) Aouani, H.; Navarro-Cia, M.; Rahmani, M.; Sidiropoulos, T. P. H.; Hong, M.; Oulton, R. F.; Maier, S. A. Multiresonant Broadband Optical Antennas as Efficient Tunable Nanosources of Second Harmonic Light. *Nano Lett.* **2012**, *12*, 4997–5002.
- (3) Gramotnev, D. K.; Bozhevolnyi, S. I. Nanofocusing of Electromagnetic Radiation. *Nat. Photonics* **2013**, *8*, 13–22.
- (4) Maier, S. A. *Plasmonics: Fundamentals and Applications*; Springer-Verlag: Berlin, 2007.
- (5) Liu, J. S. Q.; Pala, R. A.; Afshinmanesh, F.; Cai, W.; Brongersma, M. L. A Submicron Plasmonic Dichroic Splitter. *Nat. Commun.* **2011**, *2*, 525.
- (6) Curto, A. G.; Volpe, G.; Taminiau, T. H.; Kreuzer, M. P.; Quidant, R.; van Hulst, N. F. Unidirectional Emission of a Quantum Dot Coupled to a Nanoantenna. *Science* **2010**, *329*, 930–933.
- (7) Kosako, T.; Kadoya, Y.; Hofmann, H. F. Directional Control of Light by a Nano-Optical Yagi–Uda Antenna. *Nat. Photonics* **2010**, *4*, 312–315.
- (8) Bernal Arango, F.; Kwadrin, A.; Koenderink, A. F. Plasmonic Antennas Hybridized with Dielectric Waveguides. *ACS Nano* **2012**, *6*, 10156–10167.
- (9) Atwater, H. A.; Polman, A. Plasmonics for Improved Photovoltaic Devices. *Nat. Mater.* **2010**, *9*, 205–213.
- (10) Quidant, R.; Girard, C.; Weeber, J.-C.; Dereux, A. Tailoring the Transmittance of Integrated Optical Waveguides with Short Metallic Nanoparticle Chains. *Phys. Rev. B* **2004**, *69*, 085407.
- (11) Apuzzo, A.; Février, M.; Salas-Montiel, R.; Bruyant, A.; Chelnokov, A.; Léronel, G.; Dagens, B.; Blaize, S. Observation of near-Field Dipolar Interactions Involved in a Metal Nanoparticle Chain Waveguide. *Nano Lett.* **2013**, *13*, 1000–1006.
- (12) Février, M.; Gogol, P.; Aassime, A.; Mégy, R.; Delacour, C.; Chelnokov, A.; Apuzzo, A.; Blaize, S.; Lourtioz, J.-M.; Dagens, B. Giant Coupling Effect between Metal Nanoparticle Chain and Optical Waveguide. *Nano Lett.* **2012**, *12*, 1032–1037.
- (13) Sidiropoulos, T. P. H.; Maier, S. A.; Oulton, R. F. Efficient Low Dispersion Compact Plasmonic-Photonic Coupler. *Opt. Express* **2012**, *20*, 12359–12365.
- (14) Sonnefraud, Y.; Kerman, S.; Di Martino, G.; Lei, D. Y.; Maier, S. A. Directional Excitation of Surface Plasmon Polaritons via Nanoslits

under Varied Incidence Observed Using Leakage Radiation Microscopy. *Opt. Express* **2012**, *20*, 4893–4902.

(15) Lerosey, G.; Pile, D. F. P.; Matheu, P.; Bartal, G.; Zhang, X. Controlling the Phase and Amplitude of Plasmon Sources at a Subwavelength Scale. *Nano Lett.* **2009**, *9*, 327–331.

(16) Taillaert, D.; Bogaerts, W.; Bienstman, P.; Krauss, T. F.; Van Daele, P.; Moerman, I.; Verstuyft, S.; De Mesel, K.; Baets, R. An out-of-Plane Grating Coupler for Efficient Butt-Coupling between Compact Planar Waveguides and Single-Mode Fibers. *IEEE J. Quantum Electron.* **2002**, *38*, 949–955.

(17) Chen, X.; Li, C.; Tsang, H. K. Device Engineering for Silicon Photonics. *NPG Asia Mater.* **2011**, *3*, 34–40.

(18) Liao, C.-W.; Yang, Y.-T.; Huang, S.-W.; Lee, M.-C. M. Fiber-Core-Matched Three-Dimensional Adiabatic Tapered Couplers for Integrated Photonic Devices. *J. Lightwave Technol.* **2011**, *29*, 770–774.

(19) Hunsperger, R. G. *Integrated Optics: Theory and Technology*, 6th ed.; Springer, 2009.

(20) Neira, A. D.; Wurtz, G. A.; Ginzburg, P.; Zayats, A. V. Ultrafast All-Optical Modulation with Hyperbolic Metamaterial Integrated in Si Photonic Circuitry. *Opt. Express* **2014**, *22*, 10987–10994.

(21) Ang, T. W.; Reed, G. T.; Vonsovici, A.; Evans, A. G. R.; Routley, P. R.; Josey, M. R. Effects of Grating Heights on Highly Efficient Unibond SOI Waveguide Grating Couplers. *IEEE Photonics Technol. Lett.* **2000**, *12*, 59–61.

(22) Smith, C. L. C.; Thilsted, A. H.; Garcia-Ortiz, C. E.; Radko, I. P.; Marie, R.; Jeppesen, C.; Vannahme, C.; Bozhevolnyi, S. I.; Kristensen, A. Efficient Excitation of Channel Plasmons in Tailored, UV-Lithography-Defined V-Grooves. *Nano Lett.* **2014**, *14*, 1659–1664.

(23) Rukhlenko, I. D.; Premaratne, M.; Agrawal, G. P. Nonlinear Propagation in Silicon-Based Plasmonic Waveguides from the Standpoint of Applications. *Opt. Express* **2011**, *19*, 206–217.

(24) Dadap, J. I.; Espinola, R. L.; Osgood, R. M., Jr.; McNab, S. J.; Vlasov, Y. A. Spontaneous Raman Scattering in Ultrasmall Silicon Waveguides. *Opt. Lett.* **2004**, *29*, 2755.